Integrating Multiple Datasets in Google Earth Engine for Advanced Hydrological Modeling Using the Soil Conservation Service Curve Number Method

Mansoor Adil, Muhammad Azmat, Mudassir Sohail
Institute of Geographical Information System, School of Civil and Environmental Engineering, (NUST, Islamabad) Email: madil.ms21igis@student.nust.edu.pk, azmat@igis.nust.edu.pk, msohail.ms21igis@student.nust.edu.pk
***Corresponding Author:** Mansoor Adil (madil.ms21igis@student.nust.edu.pk)
Citation | Adil. M, Azmat. M, Sohail. M, "Integrating Multiple Datasets in Google Earth Engine for Advanced Hydrological Modeling Using the Soil Conservation Service Curve Number Method", IJIST, Special Issue pp 186-205, June 2024
Received | May 30, 2024 **Revised |** June 04, 2024 **Accepted |** June 08, 2024 **Published |** June 12, 2024.

This research explores the feasibility of using cloud computing and open data sources for hydrological modeling, specifically leveraging Google Earth Engine (GEE) and the Soil Conservation Service Curve Number (SCS CN) method to estimate runoff. The SCS CN approach is commonly applied in simulating rainfall-runoff processes and is effective for estimating water inflow into rivers, lakes, and streams. Google Earth Engine provides a range of functionalities, including algorithms for rapid data manipulation and visualization, and access to extensive global remote sensing and geographic information system (GIS) datasets. The study introduces an algorithm developed in GEE to analyze precipitation data and generate antecedent moisture condition (AMC) maps. This algorithm integrates MODIS land use/land cover (LULC) data with USDA soil texture data to classify hydrological soil groups. Runoff estimation utilizes three datasets: CHIRPS, GPM, and TRMM. A thorough analysis of the rainfall-runoff relationship in the Mangla watershed from 2005 to 2015 is conducted. The study quantifies runoff estimates from each dataset and performs comparative analysis to validate the accuracy and reliability of the hydrological modeling. Over the ten-year period (2005-2015), significant fluctuations in average rainfall and runoff levels are observed, with notable seasonal patterns. The highest average precipitation of 1412.194 mm occurred in 2015, resulting in an average runoff of 215.021 mm. Conversely, 2009 recorded the lowest average precipitation of 672.808 mm and an average runoff of 78.476 mm. The accuracy of the modeled runoff observations is validated using meteorological data from the Pakistan Meteorological Department (PMD), Water and Power Development Authority (WAPDA), and Climate Forecast System Reanalysis (CFSR). In 2008, 2009, and 2010, CHIRPS consistently demonstrated better accuracy compared to GPM and TRMM, with accuracies of 90%, 79%, and 86% respectively. Additionally, a sensitivity analysis of the SCS CN model parameters reveals the effects of initial abstraction and Curve Number values on runoff estimation. In conclusion, this research enhances the understanding of hydrological processes in monsoon-affected regions and offers valuable recommendations for implementing sustainable water resource management practices.

Keywords: SCS CN Method, Hydrological Modeling, Runoff Estimation, CHIRPS, GPM, TRMM, Google Earth Engine, Cloud Computing.

Introduction:

Water resources are both constrained and essential for human socioeconomic development and the survival of all living creatures. The excessive use of water, driven by population growth and development activities, puts significant stress on global water supplies. Over the past century, the rate of water extraction has increased six times faster than population growth. Physical water scarcity now affects approximately 500 million people, or one-fifth of the global population. Estimates indicate that 65% of the world's aquatic ecosystems and river outflows are at risk of degradation [1]. Most of the water needed for agricultural and domestic use comes from surface runoff. However, there have been significant global changes in surface runoff patterns [2]. The primary factors contributing to these variations are anthropogenic activities and climate change [3][4]. Anthropogenic activities include environmental disturbances caused by human actions, such as urbanization, deforestation, altered land use, and industrial and agricultural water use [5].

Runoff is a critical hydrologic variable used in numerous water resource applications. Its frequency and volume are influenced by the intensity, duration, and distribution of rainfall events. Effective watershed management requires a thorough evaluation of a watershed's hydrologic response [5]. Accurate surface runoff estimation is increasingly important in hydrology for managing water resources. Quantifying both surface and subsurface runoff is essential for various applications, including hydrologic modeling, basin water monitoring, groundwater recharge assessment, flood risk analysis, and water infrastructure design. Collecting runoff data from gauging stations is often challenging and costly. Therefore, having globally accessible, continuous, and reliable runoff data is becoming increasingly crucial.

The Natural Resources Conservation Services Curve Number (NRCS-CN) method and its variants are extensively used for estimating runoff from ungauged watersheds. Compared to earlier empirical and lumped parameter models, these methods have proven to be faster and more accurate in estimating surface runoff [6]. The hydrologic responses that lead to surface runoff are influenced by the interaction of precipitation with topography, land use, and soil characteristics. Geographic Information Systems (GIS) are advantageous for accurately quantifying surface runoff as they store and analyze the factors contributing to runoff generation. Using GIS for CN-based runoff estimation enhances the process, making it more interactive, efficient, and less labor-intensive.

The NRCS-CN approach, formerly known as the Soil Conservation Service-Curve Number (SCS-CN) method, is a well-established model for calculating rainfall runoff [7]. Developed by the USDA SCS in 1954, this method has gained popularity due to its simplicity, reliability, and ability to accommodate a wide range of parameters, including soil type, land use, surface condition, and antecedent moisture condition. Originally designed for estimating runoff from storm rainfall events in agricultural watersheds, the NRCS-CN method has been adapted for various applications, including urban hydrology, rainwater harvesting, subsurface flow estimation, evapotranspiration (ET) calculation, and rainfall-runoff modeling [8]. Its widespread use highlights its effectiveness in hydrologic applications.

Global surface runoff prediction methods often require substantial computational resources. Satellite data, available in near real-time, offer reliable estimates of surface runoff at a spatial resolution relevant to hydrology. This study presents a method for applying the NRCS-CN approach to estimate surface runoff in near real-time at pixel, watershed, regional, and global scales. Developing near real-time terrestrial time-series runoff data, especially for ungauged watersheds, is crucial for improving surface runoff and flood event estimates. Accurate runoff estimations are essential for flood predictions, hydrological engineering, agricultural planning, and water resource monitoring.

A new global dataset for curve numbers at a 250 m resolution, known as GCN250, has been recently released and made publicly available. This dataset was validated using runoff from

the Global Land Data Assimilation System (GLDAS), rather than gauge runoff data [9]. By using Google Earth Engine (GEE), a leading planetary-scale geospatial analytic tool, the dataset can be enhanced by adjusting the curve number based on its slope and cross-referencing with runoff data and real-time precipitation estimates. The GCN250 dataset, which accounts for wet, average, and dry antecedent runoff conditions, facilitates the creation of a global runoff generator [9].

The study in [10] focuses on the Darewadi watershed, employing the SCS-CN method for runoff estimation and integrating remote sensing (RS) and GIS technologies. Daily rainfall data from the Indian Meteorological Department over a 20-year period was utilized. The study demonstrates the SCS-CN model's effectiveness in calculating surface runoff depth when detailed hydrological data is not available and underscores the reliability of GIS and remote sensing in rapidly acquiring and processing data for watershed planning. The model, adapted to Indian conditions, considers variables such as soil permeability, land use, and historical soil water conditions. GIS simplifies the computation of curve numbers for runoff estimation, revealing a significant increase in maximum recharge capacity after 5 days of preceding rainfall and highlighting GIS's role in the manual calculation of curve numbers for large regions.

In [11], the modified SCS-CN approach is used to explore rainfall and runoff estimation in Khuldabad taluka, Aurangabad District, India. This study utilizes GIS and remote sensing technology to efficiently estimate runoff, considering factors like slope, vegetation cover, and watershed area. Satellite data and GIS techniques were employed to create digital databases and thematic maps, revealing varying rainfall patterns over a ten-year period (2003-2012). The computed runoff displayed variable patterns, with 2010 having the highest annual runoff. The strong correlation coefficients for daily, monthly, and annual runoff indicate the method's effectiveness, emphasizing the utility of the SCS-CN methodology and GIS technology in regional water resource management.

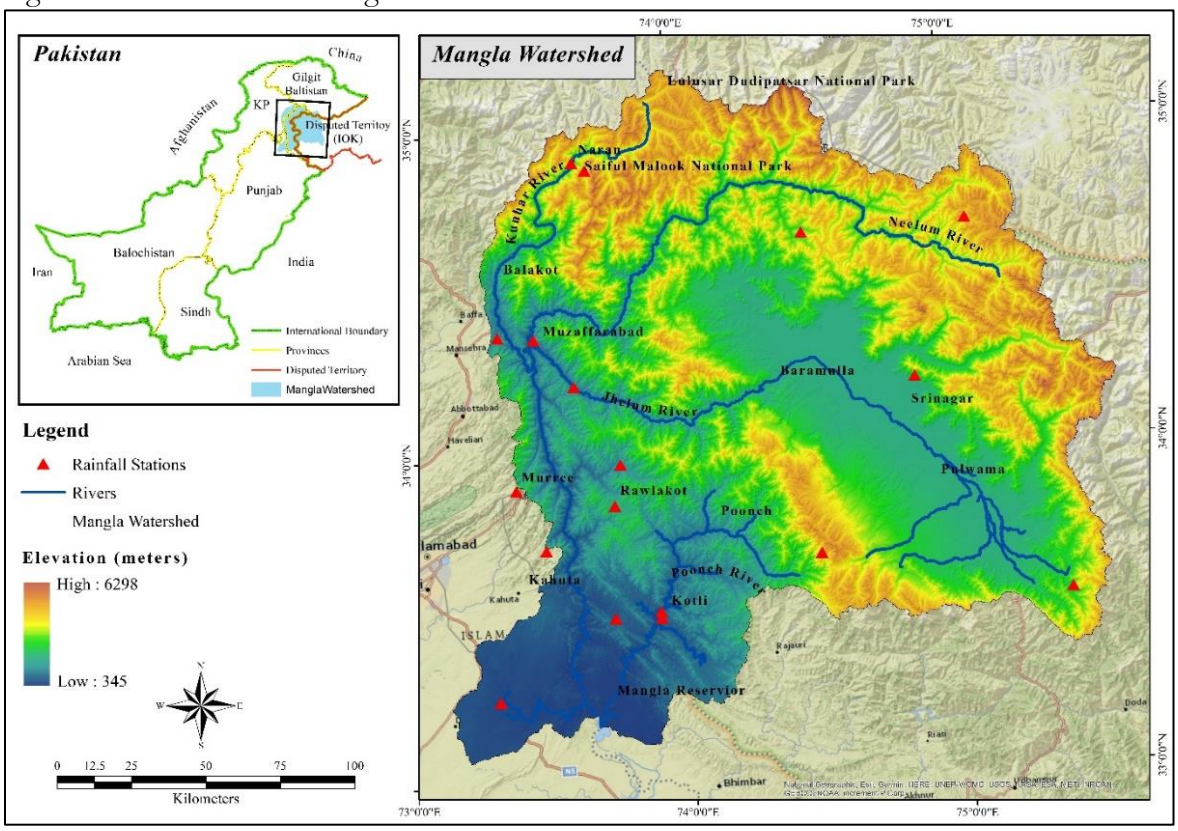

Figure 1: Study Area - Mangla Watershed

The research in [12] introduces a modified version of the SCS-CN approach to address challenges related to unexpected increases in runoff estimates. The modification improves the Soil Moisture Accounting (SMA) procedure by including storm duration, thereby enhancing accuracy and resolving structural inconsistencies. Additionally, a physical formulation for simulating soil moisture dynamics is described and validated using soil water data from an experimental plot. The revised method outperformed the original SCS-CN and [13] methods with an efficiency of 88% in both calibration and validation scenarios. The study highlights the enhanced accuracy of the modified system and suggests further research to assess its robustness and potential for simplification.

Study Area:

The Mangla Basin, located in northeast Pakistan, spans an area of 33,419 km² and is divided into seven major sub-basins: Neelum, Poonch, Kunhar, Upper Jhelum, Kanshi, Lower Jhelum, and Kahan. Each sub-basin exhibits distinct characteristics due to variations in catchment size and terrain slope [14]. The basin's hydrological dynamics are shaped by its diverse topography, which ranges from gently undulating lands to abrupt cliffs and hilly areas. The Mangla reservoir experiences a predictable seasonal inflow pattern, with the majority of water entering the reservoir between March and August, peaking in May. Conversely, from October to February, the reservoir receives relatively minimal inflow, typically less than 400 m³/s until snowmelt begins in March. This snowmelt causes a significant increase in water flow, reaching its peak in mid-May. The basin's climate is highly variable, primarily due to elevation changes [15]. As elevation increases from south to north, the climate transitions from subtropical to temperate, with temperatures falling below freezing at higher elevations. Precipitation patterns are bi-modal, with peaks in March from snowfall and in July from monsoon rains. The steep northern sections of the Kunhar sub-basin receive the highest precipitation, which significantly impacts the basin's hydrological regime [16]. Temperature variations are substantial, with summer temperatures soaring up to 50°C in the south and winter temperatures dropping below freezing in the north [17]. The Mangla Basin's distinctive terrain results from the complex interplay of hydrological processes, climate variations, and topographical factors, highlighting its critical role in water management and regional environmental sustainability [18].

Methodology:

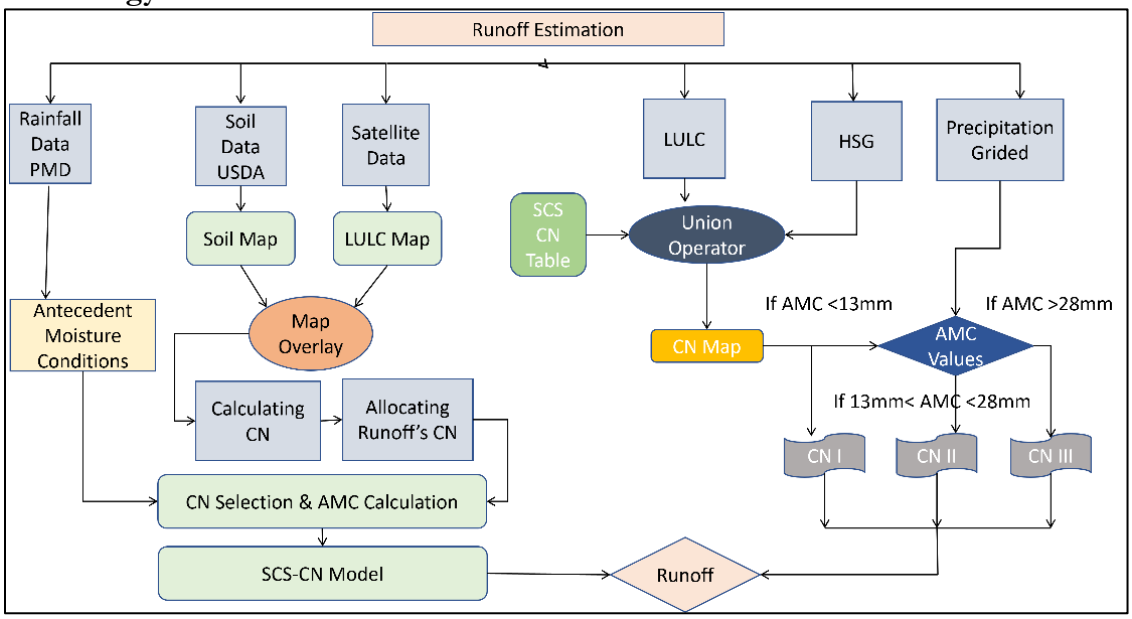

Figure 2: Methodology Flow Chart

To develop a script for the SCS CN model using cloud data and the Google Earth Engine (GEE) server, several data sources were examined for availability. The methodology was

finalized using a flowchart and script, incorporating data on land cover, rainfall (from CHIRPS, GPM, and TRMM), and soil texture (from FAO). The following image illustrates the complete process of this study.

Development of SCS CN Model:

As outlined in the Soil Conservation Service (SCS) guidelines by the National Engineering Handbook (NEH-4) Section of Hydrology [19][20], the SCS-CN model was introduced in 1954 by the USDA SCS [21]. The SCS-CN technique is based on water balance computations [22]. This event-based, lumped rainfall–runoff model is derived from the following water budget equation.

$$\mathbf{Q = \frac{(P-Ia)^2}{(P-Ia)+S}} \qquad \mathbf{P > Ia\ Equation\ i}$$

where:

Q = runoff depth, in mm
P = rainfall depth, in mm
Ia = initial abstraction, in mm
S = surface retention maximum potential, in mm

The primary components of initial abstraction include surface depression storage, initial storm infiltration, and interception. In small watersheds where lag time is minimal, initial abstraction can be inferred from observed rainfall-runoff events as the precipitation occurring before runoff begins. While surface conditions and land cover can help predict interception and surface depression storage, early-stage infiltration is highly variable, influenced by factors such as soil moisture, soil texture, and rainfall intensity. Consequently, establishing a precise relationship for estimating initial abstraction (Ia) is challenging. It is generally considered that Ia is related to \ (S \), the maximum potential surface retention. The empirical relationship between Ia and \ (S \) is expressed as follows:

$$\mathbf{Ia = 0.2S\ Equation\ ii}$$

The rainfall-runoff relationship is determined by substituting the initial abstraction value (Ia) into the discharge equation.

$$\mathbf{Q = \frac{(P-0.2S)2}{(P+0.8S)}Equation\ iii}$$

In the equation, \ (P \) represents daily rainfall, \ (Ia \) denotes the initial abstraction, \ (Q \) is the direct surface runoff, and \ (S \) signifies the potential maximum surface retention. The initial abstraction (\ (Ia \)) is calculated using \ (Ia = 0.2S \), which is used to determine the curve numbers as outlined in NEH [23].

Curve Number:

The Curve Number (CN), as defined by the U.S. Soil Conservation Service (1972), is given by:

$$\mathbf{CN = \frac{25400}{254+S}} \qquad \mathbf{for\ S\ in\ millimeters\ (mm) Equation\ iv}$$

$$\mathbf{CN = \frac{1000}{10+S}} \qquad \mathbf{for\ S\ in\ inches\ (inch) Equation\ v}$$

Where \ (S \) represents the potential maximum surface retention, and \(CN \) is a unitless runoff coefficient that depends on land use (LU), hydrological soil type, and antecedent moisture condition (AMC) [24].

The amount and duration of rainfall, soil moisture content, and land cover density all contribute to fluctuations in the Curve Number (CN). These factors collectively define the Antecedent Moisture Condition (AMC), which reflects a catchment's relative wetness or dryness and significantly impacts runoff. AMC is categorized into three classes:

- **AMC I:** Wet conditions with the lowest runoff potential
- **AMC II:** Average conditions with moderate runoff potential
- **AMC III:** Heavy rainfall with the greatest runoff potential

Antecedent moisture conditions are determined based on the antecedent rainfall over the previous five days.

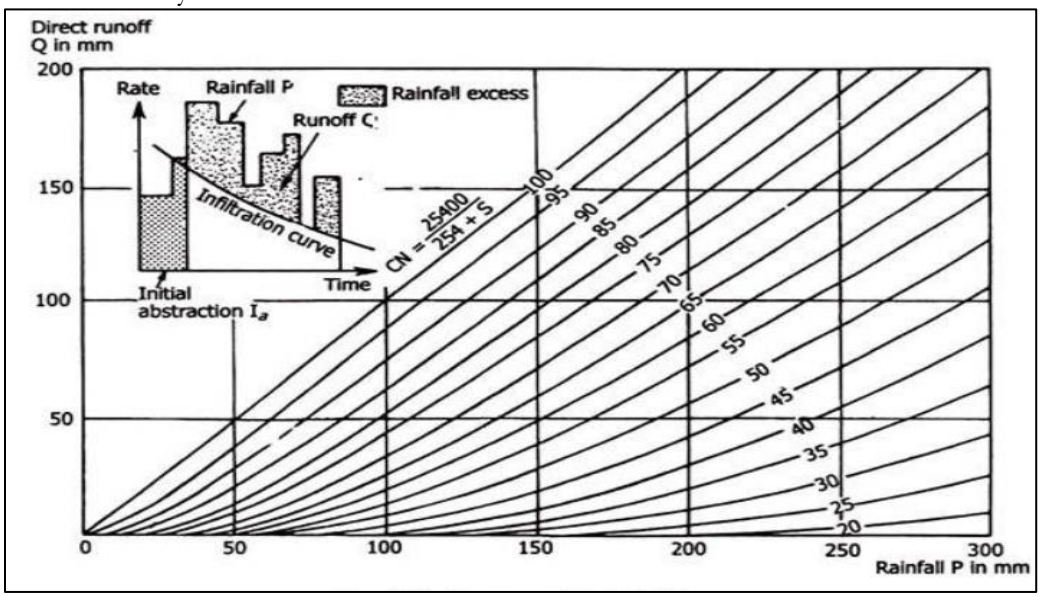

Figure 3: Curve Number Values for equation Q=(P-0.2S)2/(P+0.8S)

Table 1: AMC conditions using the 5 days antecedent rainfall.

Group	Soil Characteristics	Five-day antecedent rainfall in mm	
		Dormant Season	Growing Season
AMC I	Wet Conditions	>13	>36
AMC II	Moderate Conditions	Between 13 to 28	Between 36 to 53
AMC III	Heavy Rainfall	<28	<53

Land Use/Land Cover (LULC) and soil group conditions are combined to generate Curve Numbers (CNs) for Antecedent Moisture Condition (AMC) II. The equations used to determine CNs for AMC I and AMC III are provided below [25][26].

$$CN\ I = \frac{4.2 \times CN\ II}{10 - 0.058 \times CN\ II}$$ Equation (vi) $$CN\ III = \frac{23 \times CN\ II}{10 + 0.13 \times CN\ II}$$ Equation(vii)

The Soil Conservation Service (SCS) Curve Number (CN) model determines a soil's capacity to permit water infiltration based on Antecedent Moisture Condition (AMC) and land use/cover (LU/LC) [27]. According to the U.S. Soil Conservation Service, soils are classified into four hydrologic soil groups—A, B, C, and D—based on their infiltration rates and runoff potential. To assess the hydrological characteristics of the soil, soil texture data from the USDA Open Land Map were converted into these hydrological soil groups. Four hydrological groups (A, B, C, and D) were established from the soil texture classes, which reflect the relative proportions of sand, silt, and clay particles in the soil [28].

Table 2: The four USDA hydrologic soil groups (HSGs) are described as;

Hydrological Soil Groups	Description
HSG (A)	Sand & Sandy Loam
HSG (B)	Silty Loam & Loam
HSG (C)	Sandy Clay Loam
HSG (D)	Silt &Silty Clay Loam

A comprehensive assessment was conducted to classify land use and land cover (LULC) within the Mangla watershed. The results revealed a diverse range of land cover categories throughout the watershed. Notably, forests cover a substantial area of 9,851 square kilometers, representing 29% of the total land area. Agricultural activities are evident in the 3,311 square kilometers (10%) dedicated to crops and agricultural lands. Urban and infrastructural development is reflected in the built-up areas, which span 4,515 square kilometers (14%).

Additionally, the watershed includes 1,126 square kilometers (3%) of bare ground and 1,610 square kilometers (5%) of snow-covered regions. Vegetation remains the predominant land cover, encompassing a total area of 12,666 square kilometers, which constitutes approximately 38% of the total land area.

Table 3: Datasets Used in this research work

S/N0	Data	Type	Dataset Availability
1	TRMM, CHIRPS and GPM	Rainfall data	1998-2020
2	Open Land Map Soil Texture Class (USDA System)	Soil data	1950-2018
3	MODIS Land Cover Type Yearly Global 500m	LULC	2001-2021
4	Digital Elevation Model (SRTM)	DEM	2000
5	Station rainfall data of PMD and WAPDA	Rainfall data	1960-2020

Table 4: Mangla Watershed LuLc Area in Sq-Km

LuLc Type	Area_SqKm
Water	340
Forest	9851
Crops/Agriculture	3311
Built-up Area	4515
Bare Land	1126
Snow Covered	1610
Vegetation	12666
Total	**33419**

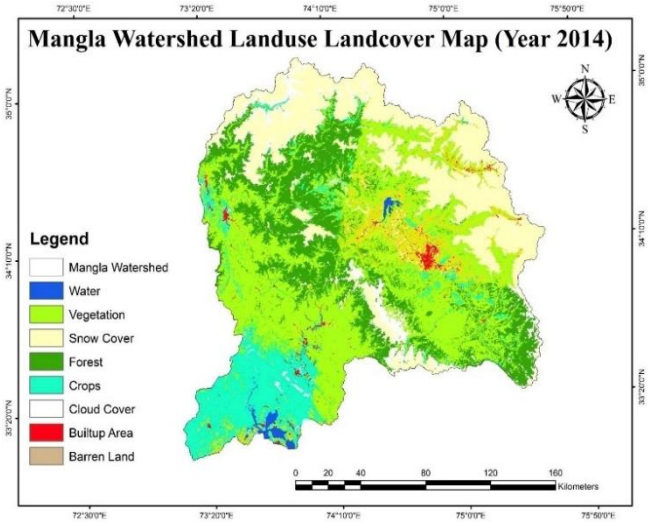

Figure 4: Mangla Watershed Land Use Land Cover Map

Mangla Watershed Soil Texture Map:

Within the study area, two distinct hydrological soil types have been identified: Group C (Sandy loam) and Group D (Clay loam). The predominant soil type in the area is Sandy loam, which features an average soil texture with a relatively even distribution of sand, silt, and clay particles. This type of soil is commonly found in regions with moderate to high levels of precipitation.

Soil data were characterized using soil texture information from the Open Land Map Soil Texture Class (USDA System) on Google Earth Engine [29]. Soil texture, which refers to the relative proportions of sand, silt, and clay particles, significantly affects soil fertility, water retention capacity, and overall soil quality.

Table 5: Hydrological Soil Group vs Runoff Potential

Hydrological Soil Group	Soil Type	Runoff Potential	Infiltration Rate mm/hr
HSG (A)	Sand & Sandy Loam	Low	Greater than 7.5
HSG (B)	Silty Loam & Loam	Medium	Between 3.8 to 7.5
HSG (C)	Sandy Clay Loam	Medium	Between 1.3 to 3.8
HSG (D)	Silt & Silty Clay Loam	High	Less than 1.3

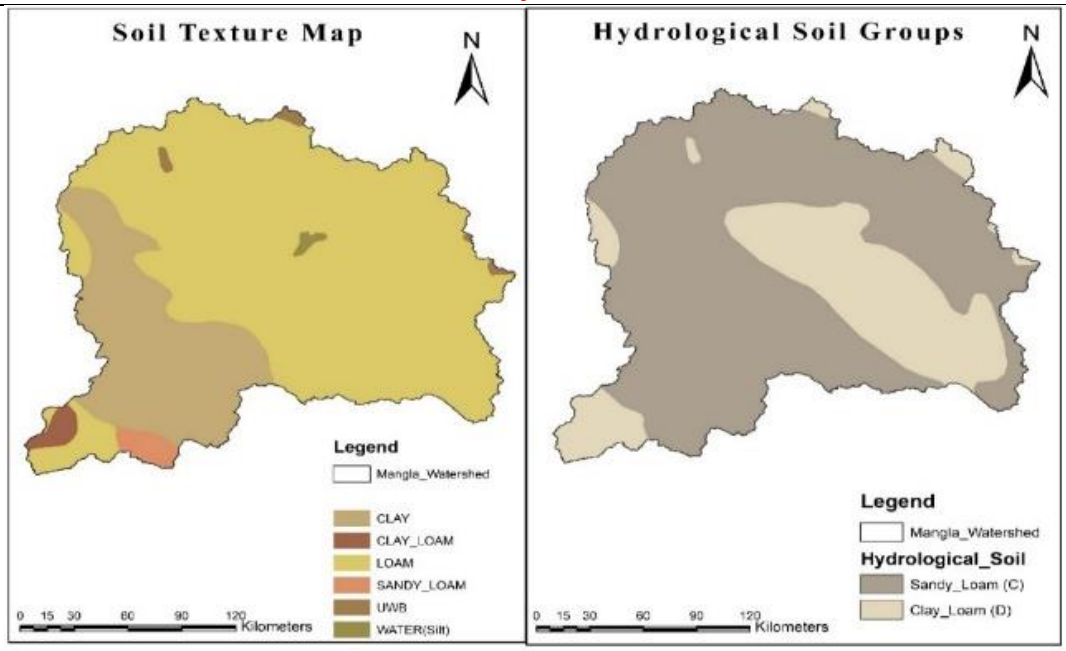

Figure 5: Mangla Watershed Soil Map

Precipitation Datasets:

In this research, we utilized three widely used rainfall datasets to analyze precipitation patterns: the Tropical Rainfall Measuring Mission (TRMM), the Global Precipitation Measurement (GPM), and the Climate Hazards Group Infrared Precipitation with Station Data (CHIRPS). CHIRPS integrates in-situ station data with satellite imagery at a resolution of 0.05°, providing precise gridded rainfall time series from 1981 to December 31, 2023 [30]. The Global Precipitation Measurement (GPM) is a groundbreaking global satellite initiative that significantly advances our understanding of precipitation patterns. Its core component, IMERG (Integrated Multi-satellite Retrievals for GPM), offers high-resolution temporal observations every three hours, capturing detailed rainfall variability [31]. The GPM mission is pivotal in global precipitation monitoring, continuously validated and developed to provide critical insights into rainfall variability and its environmental and societal impacts [32]. The TRMM dataset offers detailed insights into tropical precipitation dynamics, featuring a temporal resolution of three hours and a spatial resolution of 0.25 degrees. TRMM utilizes advanced algorithms and multiple microwave sensors to enhance and interpolate precipitation estimates, including RMS precipitation-error estimates that improve data accuracy and reliability. Understanding these datasets is crucial for comprehending the intricate relationships between tropical rainfall patterns and broader climate dynamics [33].

Generating Curve Number Map:

The Curve Number (CN) is a dimensionless parameter in hydrology that indicates the runoff potential of a watershed or specific geographical region. It is a crucial element in various hydrological models, notably the SCS-CN approach.

Table 6: CN Values for HSGs and Land Cover (USDA)

S. No	LuLc	A	B	C	D
1	Water	100	100	100	100
2	Trees	40	66	77	85
3	Terraced Crop	50	63	74	83
4	Build Up Area	81	88	91	93
5	Bare Land	68	79	86	89
6	Snow/Ice	98	98	98	98
7	Vegetation	63	77	88	88

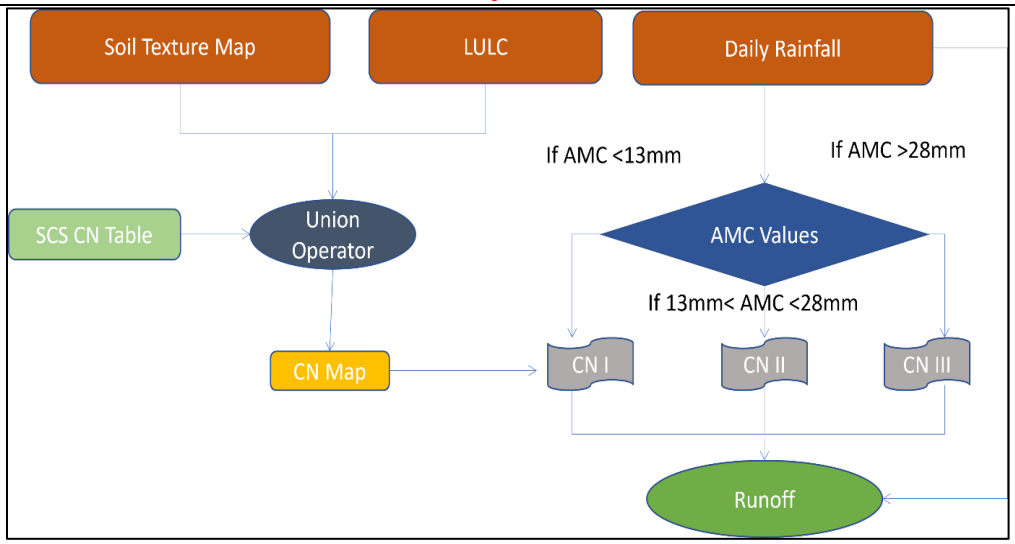

Figure 6: Google Earth Engine Flow Chart [34].

SCS CN Model in GEE:

Google Earth Engine's extensive collection of spatial data facilitates the selection of input data through various filtering methods, enabling users to refine datasets from large image collections. Unlike current models, GEE can handle dynamic data efficiently. The process begins with using a ternary operator to classify the soil texture map into four hydrologic soil groups (A, B, C, and D). Following this, a conditional statement is employed to generate the Curve Number (CN II) map for each combination of the four soil groups and the 17 MODIS Land Use/Land Cover (LULC) datasets. The CN I and CN III maps are then derived from CN II using the respective equations. The S image, which depends on the Antecedent Moisture Condition (AMC), serves a similar purpose to the CN image. Consequently, the S values for the CN maps are calculated during the final runoff (Q) computation. To optimize processing time, the script creates S images as a global variable applicable to all CN conditions [34].

Create CN Map using JavaScript Expression:

The CN values assigned to individual pixels were evaluated for accuracy using the inspector tool to ensure the reliability of the CN map. This involved verifying that the assigned CN values aligned with the expected values for each land use/land cover and soil hydrological group, as outlined in the CN table provided by the United States Department of Agriculture (USDA). For instance, water bodies should have CN values ranging from 98 to 100. The inspector tool revealed that water bodies had a CN value of 100, thereby confirming the accuracy of the generated CN values.

Table 7: Curve Number Expression using "IF" Statement

Soil Group A	Soil Group C
(a('soil') = 1) && (a('lulc') =1) 35	(c('soil') = 3) && (c('lulc') =1) 73
(a('soil') = 1) && (a('lulc') =2) 25	(c('soil') = 3) && (c('lulc') =2) 70
(a('soil') = 1) && (a ('lulc' =3) 45	(c('soil') = 3) && (c('lulc' =3) 77
(a('soil') = 1) && (a('lulc') =4) 39	(c('soil') = 3) && (c('lulc') =4) 74
(a('soil') = 1) && (a('lulc') =5) 45	(c('soil') = 3) && (c('lulc') =5) 77
(a('soil') = 1) && (a('lulc') =6) 49	(c('soil') = 3) && (c('lulc') =6) 79
(a('soil') = 1) && (a('lulc') =7) 68	(c('soil') = 3) && (c('lulc') =7) 86
(a('soil') = 1) && (a('lulc') =8) 36	(c('soil') = 3) && (c('lulc') =8) 73
(a('soil') = 1) && (a('lulc') =9) 45	(c('soil') = 3) && (c('lulc') =9) 77
(a('soil') = 1) && (a('lulc') =10) 30	(c('soil') = 3) && (c('lulc') =10) 71
(a('soil') = 1) && (a('lulc') =11) 95	(c('soil') = 3) && (c('lulc') =11) 96
(a('soil') = 1) && (a('lulc') =12) 66	(c('soil') = 3) && (c('lulc') =12) 85

(a('soil') = 1) && (a('lulc') =13) 72	(c('soil') = 3) && (c('lulc') =13) 87
(a('soil') = 1) && (a('lulc') =14) 63	(c('soil') = 3) && (c('lulc') =14) 83
(a('soil') = 1) && (a('lulc') =15) 100	(c('soil') = 3) && (c('lulc') =15) 100
(a('soil') = 1) && (a('lulc') =16) 73	(c('soil') = 3) && (c('lulc') =16) 90
(a('soil') = 1) && (a('lulc') =17) 100	(c('soil') = 3) && (c('lulc') =17) 100
Soil Group B	**Soil Group D**
(b('soil') = 2) && (b('lulc') =1) 51	(d('soil') = 4) && (d('lulc') =1) 78
(b('soil') = 2) && (b('lulc') =2) 55	(d('soil') = 4) && (d('lulc') =2) 77
(b('soil') = 2) && (b ('lulc' =3) 66	(d('soil') = 4) && (d ('lulc' =3) 82
(b('soil') = 2) && (b('lulc') =4) 61	(d('soil') = 4) && (d('lulc') =4) 81
(b('soil') = 2) && (b('lulc') =5) 66	(d('soil') = 4) && (d('lulc') =5) 82
(b('soil') = 2) && (b('lulc') =6) 69	(d('soil') = 4) && (d('lulc') =6) 90
(b('soil') = 2) && (b('lulc') =7) 79	(d('soil') = 4) && (d('lulc') =7) 89
(b('soil') = 2) && (b('lulc') =8) 60	(d('soil') = 4) && (d('lulc') =8) 79
(b('soil') = 2) && (b('lulc') =9) 65	(d('soil') = 4) && (d('lulc') =9) 83
(b('soil') = 2) && (b('lulc') =10) 58	(d('soil') = 4) && (d('lulc') =10) 78
(b('soil') = 2) && (b('lulc') =11) 95	(d('soil') = 4) && (d('lulc') =11) 95
(b('soil') = 2) && (b('lulc') =12) 78	(d('soil') = 4) && (d('lulc') =12) 89
(b('soil') = 2) && (b('lulc') =13) 81	(d('soil') = 4) && (d('lulc') =13) 89
(b('soil') = 2) && (b('lulc') =14) 75	(d('soil') = 4) && (d('lulc') =14) 87
(b('soil') = 2) && (b('lulc') =15) 100	(d('soil') = 4) && (d('lulc') =15) 100
(b('soil') = 2) && (b('lulc') =16) 84	(d('soil') = 4) && (d('lulc') =16) 92
(b('soil') = 2) && (b('lulc') =17) 100	(d('soil') = 4) && (d('lulc') =17) 100

Rainfall:

After generating the Curve Number (CN) map, three rainfall datasets were utilized to evaluate the hydrological modeling process. These datasets were integrated with the CN map to enhance the modeling approach.

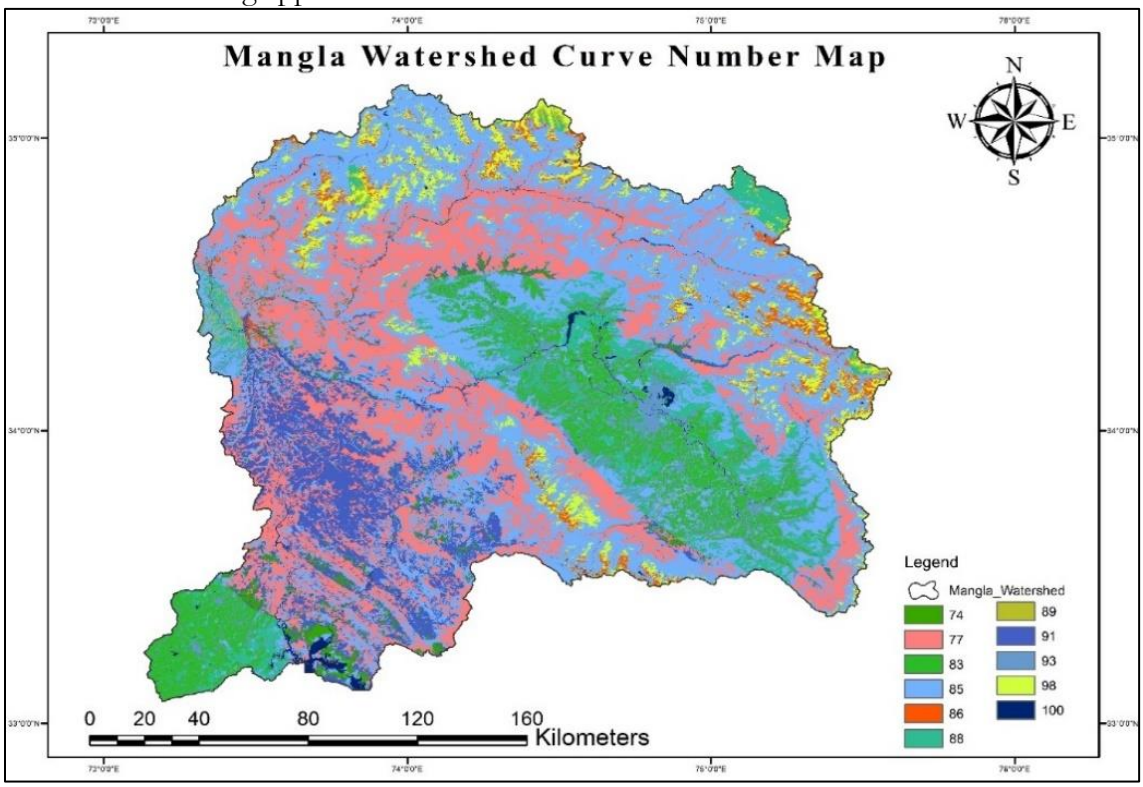

Figure 7: Mangla Watershed Curve Number Map

The Climate Hazards Group InfraRed Precipitation with Station Data (CHIRPS) daily dataset [35] was employed first, followed by the Global Precipitation Measurement (GPM) [32] and Tropical Rainfall Measuring Mission (TRMM) [36] datasets. CHIRPS data, with a temporal resolution of 24 hours, was combined with TRMM and GPM data, which are available every three hours. To ensure consistency in the analysis, TRMM and GPM data were converted to daily values using mathematical computations.

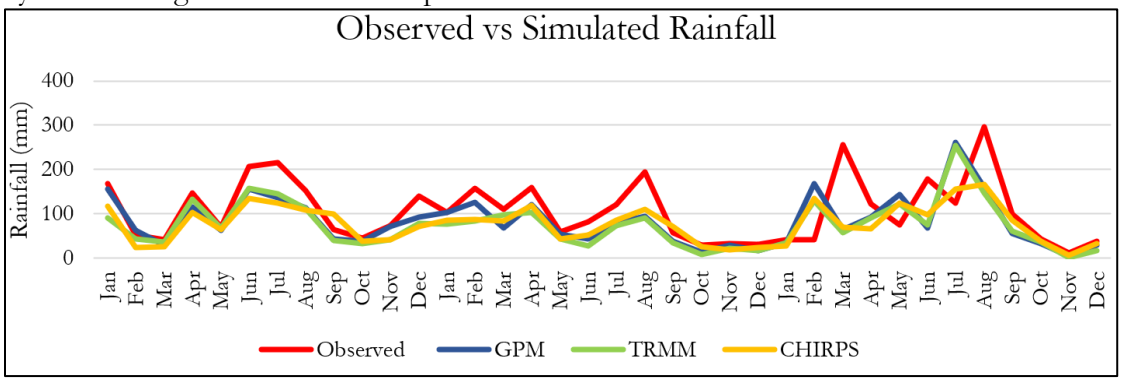

Figure 8: Observed vs Simulated Rainfall Graph

Daily Antecedent Moisture Condition (AMC) images were generated based on rainfall data. First, the AMC value range for each pixel and day was examined. A Soil Moisture Condition (S) image was then created based on each pixel's AMC value. Specifically, pixels with AMC values less than 13 mm were replaced with values from the S-I image computed using CN I [40], while pixels with AMC values greater than 28 mm were replaced with values from the S-III image computed using CN III. According to [40], pixels with AMC values between 13 and 28 mm retained their CN II values. This approach allowed for the creation of a single S image per day, reflecting the appropriate soil moisture levels based on AMC values across the study area. The S image served as the foundation for further hydrological modeling and analysis, offering insights into the interplay between runoff potential, soil moisture, and rainfall.

Table 8: Inventory of Climate stations

No.	Station Name	Latitude N	Longitude E	Elevation(m)	Data Source	Data Availability
1	Balakot	34.38	73.35	995	PMD	1962-2023
2	Ghari Dopatta	34.22	73.62	814	PMD	1961-2023
3	Kotli	33.52	73.90	614	PMD	1981-2023
4	Murree	33.90	73.39	2213	PMD	1961-2023
5	Muzaffarabad	34.37	73.48	686	PMD	1961-2023
6	Bagh	33.97	73.77	1067	WAPDA	1970-2009
7	Domel	33.71	73.49	702	WAPDA	1970-2009
8	Gujjar Khan	33.26	73.30	547	WAPDA	1970-2009
9	Naran	34.90	73.64	2362	WAPDA	1970-2009
10	Rawalakot	33.85	73.75	1676	WAPDA	1970-2009
11	Rehman Bridge	33.50	73.90	530	WAPDA	1970-2009
12	Saiful Maluk	34.88	73.69	3240	WAPDA	1970-2009
13	Sehr Kokata	33.50	73.73	915	WAPDA	1970-2009
14	Neelum	34.66	74.47	1035	CFSR	2000-2022
15	Baramulla	34.68	75.07	995	CFSR	2000-2022
16	Srinagar	34.20	74.86	1050	CFSR	2000-2022
17	Pulwama	33.67	74.49	1102	CFSR	2000-2022
18	Poonch	33.53	75.39	802	CFSR	2000-2022

*CFSR [37][38][39]

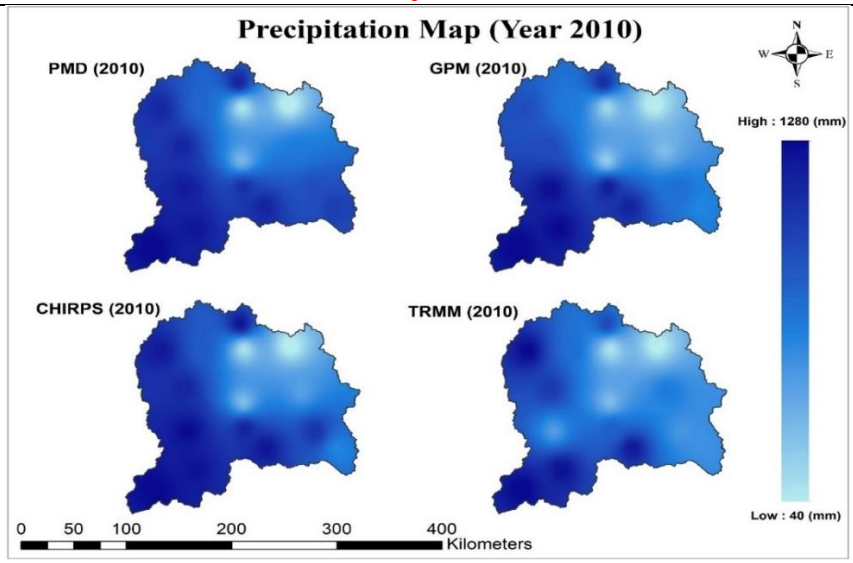

Figure 9: Rainfall Spatial Maps (Year 2010)

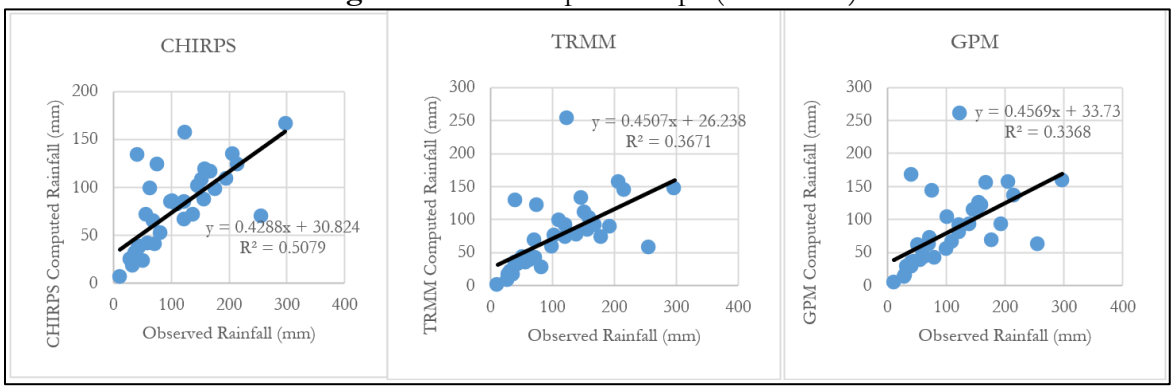

Figure 10: CHIRPS, TRMM and GPM Computed vs Observed Rainfall

Results and Discussions:

The rainfall-runoff model was effectively developed on the Google Earth Engine (GEE) platform using the Soil Conservation Service Curve Number (SCS-CN) method. This model leverages GEE's JavaScript API to integrate critical datasets, including rainfall data, land use/land cover (LULC) maps, and soil maps. To create Curve Number (CN) maps, the soil texture map was first categorized into hydrological soil groups and then combined with LULC data. Antecedent Moisture Conditions (AMC) were assessed based on the precipitation received over the previous five days. Daily runoff was subsequently calculated, taking into account the AMC conditions for each pixel.

The study area covered the Mangla watershed over a ten-year period from 2005 to 2015. It is crucial to note that the study operates under the assumption that rainfall should always exceed runoff. Instances where runoff exceeds rainfall suggest potential calculation errors. Analyzing the CHIRPS, GPM, and TRMM datasets from 2005 to 2015 provides valuable insights into summer monsoon rainfall patterns in the Mangla watershed. The datasets reveal distinct seasonal variations and overall trends, highlighting the unpredictability of the monsoon with significant year-to-year variability. Despite differences between datasets, they consistently depict the seasonal onset and withdrawal of the monsoon, with peak rainfall during the monsoon months. Figure-10 illustrates yearly rainfall compared to runoff values for each dataset. In 2005, GPM recorded the highest rainfall at 944.98 mm, resulting in a mean runoff of 83.83 mm, while CHIRPS showed a mean rainfall of 905.75 mm with a runoff of 179.87 mm. TRMM recorded the lowest rainfall of 838.62 mm for the same year, resulting in a mean runoff of 127.20 mm. Despite significant rainfall, GPM produced only 8.8% runoff due to a dry monsoon season, with

just 293 mm of rainfall leading to AMC I (lowest runoff potential). In 2006, rainfall increased notably, with GPM recording 1283.32 mm of mean precipitation and a runoff of 242.89 mm, a 44% increase in runoff. TRMM reported a mean rainfall of 1140.19 mm, yielding a runoff of 210.77 mm, while CHIRPS observed 1002.14 mm of rainfall with a runoff of 241.74 mm. From 2007 to 2009, rainfall levels were relatively stable, with CHIRPS recording mean rainfalls of 932.36 mm in 2007, 948.24 mm in 2008, and 800.15 mm in 2009, producing corresponding runoffs of 210.80 mm, 202.97 mm, and 119.12 mm. For GPM, rainfall was 867.92 mm in 2007, 1078.83 mm in 2008, and 782.78 mm in 2009, with runoffs of 124 mm, 140 mm, and 63.24 mm, respectively.

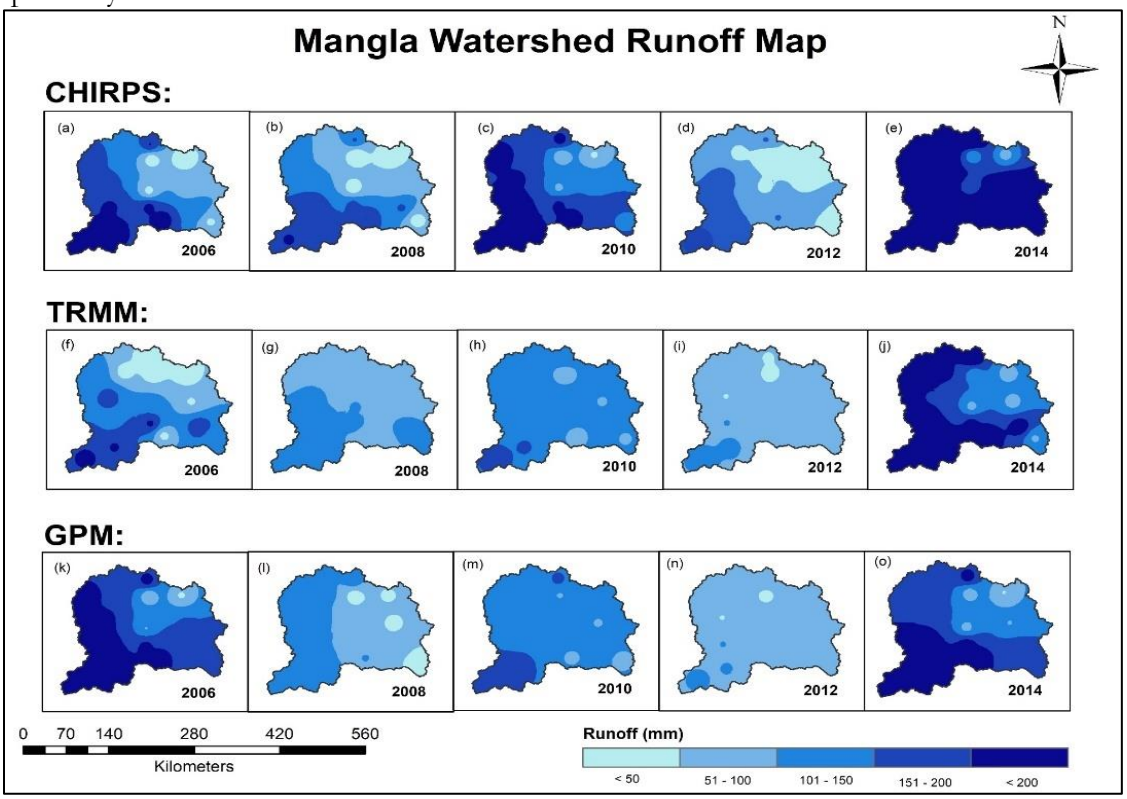

Figure 11: CHIRPS, TRMM and GPM Runoff Maps

In 2010, a slight increase in rainfall led to higher runoff values. CHIRPS recorded a mean runoff of 230.63 mm, TRMM 159.13 mm, and GPM 173.06 mm. The following three years (2011-2013) were relatively dry, with GPM, TRMM, and CHIRPS each reporting a mean rainfall of 876.88 mm, resulting in a mean runoff of 132.20 mm. In 2014, characterized by heavy monsoon rains, high precipitation values were recorded: CHIRPS at 1244.06 mm, TRMM at 1098.22 mm, and GPM at 1170.56 mm, resulting in mean runoffs of 402.65 mm, 285.20 mm, and 254.09 mm, respectively. In 2015, a rich pre-monsoon season was noted, with CHIRPS recording 1228.06 mm of rainfall and a runoff of 283.82 mm. TRMM and GPM recorded mean rainfalls of 1175.79 mm and 1412.19 mm, respectively, with corresponding runoffs of 287.36 mm and 215.02 mm. Overall, there was an increasing trend in rainfall values across all datasets from 2005 to 2015. GPM consistently led in rainfall measurements, while CHIRPS showed dominance in runoff values, with TRMM transitioning between the two.

Monsoon:

The Indus River basin experiences two primary sources of rainfall: the monsoon and western disturbances [41]. Western disturbances typically occur from December to March, while the monsoon season spans from June to September. The Indian Monsoon, also known as the summer monsoon in South Asia, significantly influences regional weather patterns and agricultural practices [42]. It provides relief from the extreme heat preceding the monsoon,

which lasts from June to September. Countries such as Pakistan [43], India, Bangladesh, and Nepal rely heavily on the summer monsoon for annual rainfall, which supports agricultural activities and replenishes groundwater reserves [44].

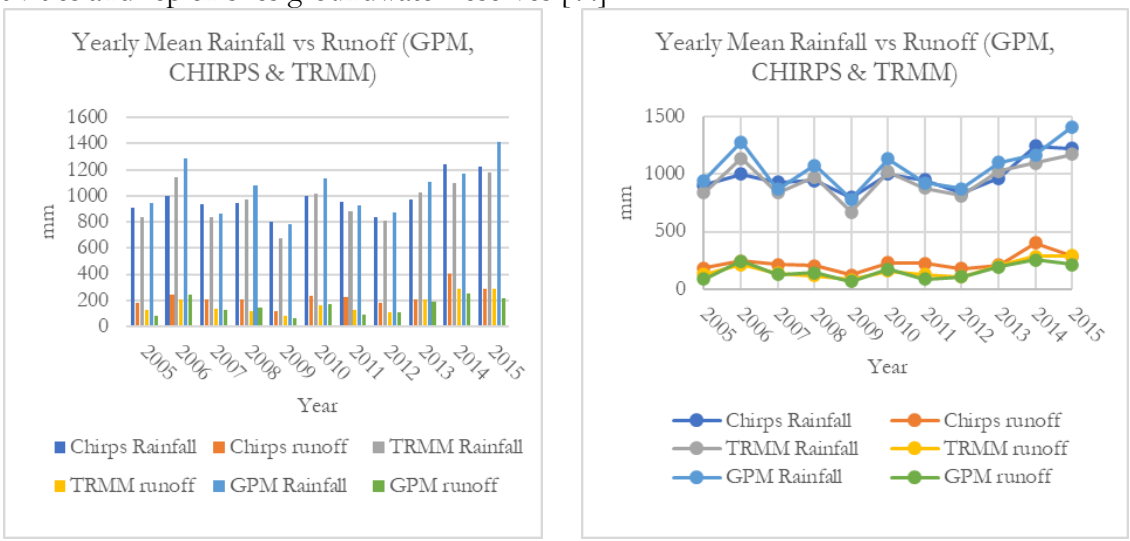

Figure 12: Yearly Rainfall vs Runoff (GPM, TRMM & CHIRPS)

To examine seasonal variations in precipitation over the Mangla watershed, we compared precipitation characteristics between TRMM, GPM, and CHIRPS for three selected years: 2006, 2010, and 2015. These years were chosen due to their significant rainfall patterns. Figure 11 displays the runoff values recorded for each rainfall dataset during the monsoon season, highlighting differences in runoff generation. For instance, in June 2006, CHIRPS recorded an average runoff of 20 mm, GPM 3.4 mm, and TRMM 3.5 mm. During the peak monsoon months of July and August, CHIRPS recorded runoff values of 125 mm in 2006, 112 mm in 2010, and 73 mm in 2015. GPM recorded 146 mm, 105 mm, and 43 mm for the same years, while TRMM showed 122 mm, 80 mm, and 42 mm. Overall, CHIRPS exhibited the highest total runoff during the peak monsoon season, followed by GPM, with TRMM showing the lowest runoff values.

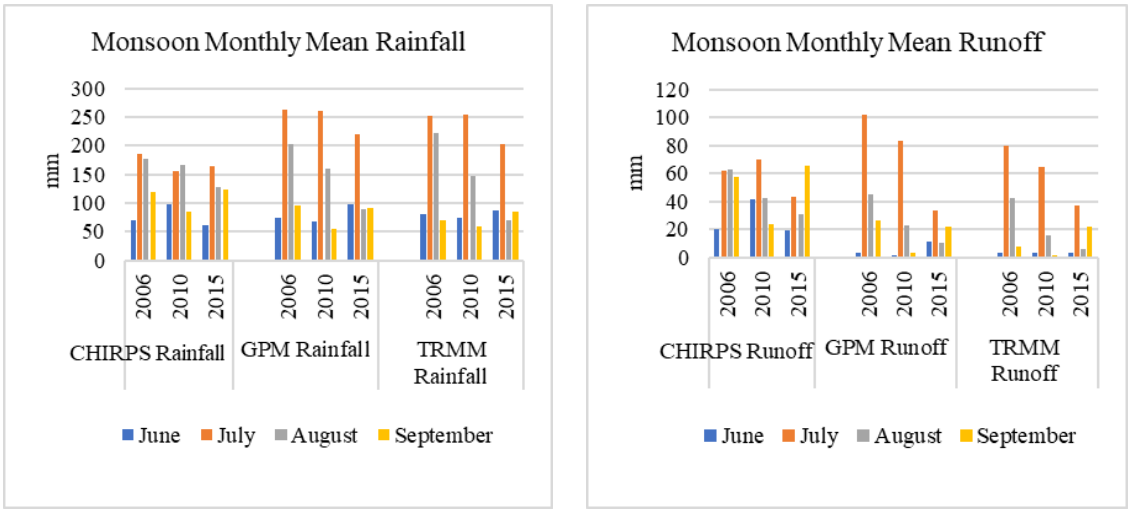

Figure 13: TRMM, GPM and CHIRPS Monsoon Rainfall and Runoff

Year-to-year variations in seasonal mean monsoon rainfall for 2006, 2010, and 2015 were compared among TRMM, GPM, and CHIRPS datasets. In 2006, GPM recorded the highest mean rainfall of 637 mm, followed by TRMM with 623 mm, and CHIRPS with the lowest at 552 mm. Interestingly, despite the lowest rainfall recorded by CHIRPS in 2006, it exhibited the highest runoff of 202 mm, compared to 176 mm for GPM and 133 mm for TRMM. This high

runoff in CHIRPS was due to AMC III conditions, characterized by consistent rainfall and high soil moisture content, indicating the highest runoff potential. For the 2010 monsoon season, CHIRPS recorded a mean rainfall of 505 mm, resulting in a mean runoff of 176 mm. In contrast, GPM observed a mean rainfall of 543 mm, generating a runoff of 111 mm, while TRMM had a mean rainfall of 535 mm and a runoff of only 85 mm. In 2015, CHIRPS reported a mean rainfall of 478 mm, leading to a mean runoff of 158 mm. GPM recorded a higher mean rainfall of 499 mm but had a lower runoff of 77 mm. TRMM showed the lowest mean precipitation of 443 mm and a corresponding runoff of 67 mm.

Results Validation:

To validate the results, daily meteorological data from 1961 to 2022 were obtained from the Pakistan Meteorological Department (PMD), Water and Power Development Authority (WAPDA), and Climate Forecast System Reanalysis (CFSR). While WAPDA stations primarily observe flow discharge data, they also record some climatic data, including precipitation and temperature. An inventory of meteorological stations is detailed in Table-7. Given that the Mangla Basin is a transboundary waterbody and the data from PMD and WAPDA do not cover the entire basin, CFSR data were used in conjunction with PMD and WAPDA data for validation purposes. CFSR data are particularly useful in data-scarce regions [38]. Of the 18 stations used for validation, data from five stations were sourced from the CFSR database.

For the year 2008, the actual mean runoff calculated from ground stations was 224.96 mm, while the observed mean runoff for CHIRPS was 202.9 mm, reflecting an accuracy of 90%. For GPM, the mean runoff observed was 140.5 mm, with an accuracy of 62.5%, and for TRMM, the mean runoff was 117 mm, resulting in the lowest accuracy of 52%. In 2009, the actual runoff recorded was 149.71 mm, with CHIRPS showing an observed runoff of 119.12 mm (79% accuracy), GPM 78.47 mm (52% accuracy), and TRMM 63.24 mm (42% accuracy). For the year 2010, the recorded mean runoff was 267.37 mm. The observed runoff values were 230.63 mm for CHIRPS, 173.064 mm for GPM, and 159.19 mm for TRMM, with CHIRPS demonstrating the highest accuracy at 86%, followed by GPM with 65% accuracy, and TRMM with approximately 60% accuracy.

Sensitivity Analysis:

The SCS CN model equation clearly requires only two input parameters: the initial abstraction value and the rainfall data.

$$\mathbf{Q = \frac{(P - Ia)^2}{(P - Ia) + S}}$$

Where,

$$\mathbf{Ia = 0.2S}$$

$$\mathbf{Q = \frac{(P - 0.2S)2}{(P + 0.8S)}} \quad \text{Equation(a)}$$

$$\mathbf{CN = \frac{25400}{254 + S}} \quad \textbf{for S in millimeters (mm)}$$

From Equation (a), it is evident that basin recharge (S) is dependent on the Curve Number (CN) value. We evaluated the model's sensitivity to variations in CN and S values. As shown in Figure 12, the estimated runoff was zero when CN values were below 70. Runoff values increased with higher CN values, reaching the level of rainfall at CN=100, which corresponds to water bodies. Conversely, Figure 12 demonstrates that runoff values gradually decrease as initial abstraction (Ia) values increase. Higher Ia values result in lower estimated runoff, and vice versa. This comparative analysis confirms that the SCS CN model is more sensitive to changes in CN values than to changes in Ia values, a finding supported by previous research [45].

Table 9: Results Validation against each Watershed

Objectid	Shape	LULC	Watershed	hydgrp	CN	Basin Recharge	Ia =0.2S
273523	Polygon	Built-up	WS-1	C	91	25.12088	5.024176
274025	Polygon	Vegetations	WS-1	C	85	44.82353	8.964706
274233	Polygon	Crops	WS-1	C	74	89.24324	17.84865
274980	Polygon	Barren Land	WS-1	C	86	41.34884	8.269768
275568	Polygon	Crops	WS-1	C	74	89.24324	17.84865
275615	Polygon	Trees	WS-1	C	77	75.87013	15.17403
381596	Polygon	Snow/Ice	WS-2	C	98	5.183673	1.036735
381683	Polygon	Trees	WS-2	C	77	75.87013	15.17403
381746	Polygon	Vegetations	WS-2	C	85	44.82353	8.964706
383132	Polygon	Barren Land	WS-2	C	86	41.34884	8.269768
384209	Polygon	Water	WS-2	C	100	0	0
263	Polygon	Snow/Ice	WS-3	C	98	5.183673	1.036735
264	Polygon	Barren Land	WS-3	C	86	41.34884	8.269768
269	Polygon	Vegetations	WS-3	C	85	44.82353	8.964706
1264	Polygon	Barren Land	WS-4	D	89	31.39326	6.278652
1837	Polygon	Snow/Ice	WS-4	D	98	5.183673	1.036735
2555	Polygon	Vegetations	WS-4	D	88	34.63636	6.927272
2084	Polygon	Snow/Ice	WS-4	C	98	5.183673	1.036735
2158	Polygon	Barren Land	WS-4	C	86	41.34884	8.269768
2567	Polygon	Vegetations	WS-4	C	85	44.82353	8.964706
127942	Polygon	Snow/Ice	WS-5	C	98	5.183673	1.036735
129938	Polygon	Vegetations	WS-5	C	85	44.82353	8.964706
130065	Polygon	Built-up	WS-5	C	91	5.183673	1.036735
130422	Polygon	Trees	WS-5	C	77	75.87013	15.17403
131274	Polygon	Water	WS-5	C	100	0	0
156846	Polygon	Barren Land	WS-6	C	86	41.34884	8.269768
157475	Polygon	Trees	WS-6	C	77	75.87013	15.17403
157571	Polygon	Vegetations	WS-6	C	85	44.82353	8.964706
160555	Polygon	Snow/Ice	WS-6	C	98	5.183673	1.036735
173402	Polygon	Water	WS-6	C	100	0	0
167119	Polygon	Crops	WS-6	C	74	89.24324	17.84865
175467	Polygon	Trees	WS-6	D	85	44.82353	8.964706
175806	Polygon	Vegetations	WS-6	D	88	34.63636	6.927272
176128	Polygon	Snow/Ice	WS-6	D	98	5.183673	1.036735

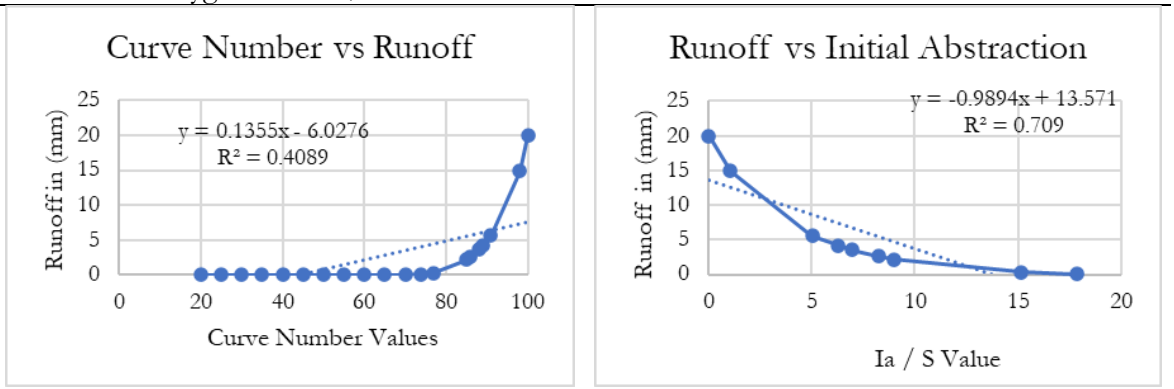

Figure 14: Runoff vs Curve Number and Runoff vs Initial Abstriction

Conclusion and Recommendations:

The application of Geographic Information Systems (GIS) in hydrologic modeling and water resource management is essential for effectively analyzing and managing large datasets related to water resources. However, processing these extensive datasets requires considerable computing power, which can be a challenge for traditional computing environments. To address this, the developed runoff model utilizes the robust computing capabilities of Google Earth Engine. Google Earth Engine offers a scalable platform that enables the processing of big data within minutes [46], overcoming the limitations of conventional computing resources and significantly reducing the time required for modeling. The runoff model incorporates various data inputs, such as soil data, land cover data, rainfall data, and Antecedent Moisture Conditions (AMC). Nonetheless, it is important to recognize that the model's default Curve Number (CN) for water bodies and snow may not always accurately represent their hydrological characteristics. While a CN of 98-100 may be suitable for water bodies, it is not ideal for snow-covered terrain.

To improve the model's accuracy, it is recommended to adjust the CN values for snow-covered areas by considering additional factors such as temperature, which plays a crucial role in snowmelt processes. Including temperature data allows for the calculation of growing degree days or melting degree days, which can be used to derive more precise CN values for snow-covered terrain. By refining the CN values based on temperature data, the runoff model can provide more realistic simulations of hydrological processes in snow-covered regions, thereby enhancing the efficiency of hydrologic modeling and water resource management.

References:

[1] W. Shi and N. Wang, "An Improved SCS-CN Method Incorporating Slope, Soil Moisture, and Storm Duration Factors for Runoff Prediction," Water 2020, Vol. 12, Page 1335, vol. 12, no. 5, p. 1335, May 2020, doi: 10.3390/W12051335.

[2] N. Gedney, P. M. Cox, R. A. Betts, O. Boucher, C. Huntingford, and P. A. Stott, "Detection of a direct carbon dioxide effect in continental river runoff records," Nat. 2006 4397078, vol. 439, no. 7078, pp. 835–838, Feb. 2006, doi: 10.1038/nature04504.

[3] H. Chu, J. Wei, J. Qiu, Q. Li, and G. Wang, "Identification of the impact of climate change and human activities on rainfall-runoff relationship variation in the Three-River Headwaters region," Ecol. Indic., vol. 106, p. 105516, Nov. 2019, doi: 10.1016/J.ECOLIND.2019.105516.

[4] Y. Xu, S. Wang, X. Bai, D. Shu, and Y. Tian, "Runoff response to climate change and human activities in a typical karst watershed, SW China," PLoS One, vol. 13, no. 3, p. e0193073, Mar. 2018, doi: 10.1371/JOURNAL.PONE.0193073.

[5] N. Akhtar, M. I. Syakir Ishak, S. A. Bhawani, and K. Umar, "Various Natural and Anthropogenic Factors Responsible for Water Quality Degradation: A Review," Water 2021, Vol. 13, Page 2660, vol. 13, no. 19, p. 2660, Sep. 2021, doi: 10.3390/W13192660.

[6] S. K. Mishra and V. P. Singh, "Validity and extension of the SCS-CN method for computing infiltration and rainfall-excess rates," Hydrol. Process., vol. 18, no. 17, pp. 3323–3345, Dec. 2004, doi: 10.1002/HYP.1223.

[7] M. Lal et al., "Evaluation de la méthode du numéro de courbe du Service de la Conservation des Sols à partir de données provenant de parcelles agricoles," Hydrogeol. J., vol. 25, no. 1, pp. 151–167, Feb. 2017, doi: 10.1007/S10040-016-1460-5/METRICS.

[8] S. Verma, R. K. Verma, S. K. Mishra, A. Singh, and G. K. Jayaraj, "A revisit of NRCS-CN inspired models coupled with RS and GIS for runoff estimation," Hydrol. Sci. J., vol. 62, no. 12, pp. 1891–1930, Sep. 2017, doi: 10.1080/02626667.2017.1334166.

[9] L. H. Sujud and H. H. Jaafar, "A global dynamic runoff application and dataset based on

the assimilation of GPM, SMAP, and GCN250 curve number datasets," Sci. Data 2022 91, vol. 9, no. 1, pp. 1–11, Nov. 2022, doi: 10.1038/s41597-022-01834-0.

[10] A. W. Dhawale, "Runoff Estimation for Darewadi Watershed using RS and GIS 47", [Online]. Available: https://www.ijrte.org/wp-content/uploads/papers/v1i6/F0413021613.pdf

[11] "Estimation of Runoff by using SCS Curve Number Method and Arc GIS." Accessed: Jun. 16, 2024. [Online]. Available: https://www.researchgate.net/publication/290947015_Estimation_of_Runoff_by_using_SCS_Curve_Number_Method_and_Arc_GIS

[12] W. Shi and N. Wang, "Improved SMA-based SCS-CN method incorporating storm duration for runoff prediction on the Loess Plateau, China," Hydrol. Res., vol. 51, no. 3, pp. 443–455, Jun. 2020, doi: 10.2166/NH.2020.140.

[13] P. K. Singh, S. K. Mishra, R. Berndtsson, M. K. Jain, and R. P. Pandey, "Development of a Modified SMA Based MSCS-CN Model for Runoff Estimation," Water Resour. Manag., vol. 29, no. 11, pp. 4111–4127, Sep. 2015, doi: 10.1007/S11269-015-1048-1/METRICS.

[14] H. Haider et al., "Appraisal of Climate Change and Its Impact on Water Resources of Pakistan: A Case Study of Mangla Watershed," Atmos. 2020, Vol. 11, Page 1071, vol. 11, no. 10, p. 1071, Oct. 2020, doi: 10.3390/ATMOS11101071.

[15] U. W. Humphries et al., "Runoff Estimation Using Advanced Soft Computing Techniques: A Case Study of Mangla Watershed Pakistan," Water 2022, Vol. 14, Page 3286, vol. 14, no. 20, p. 3286, Oct. 2022, doi: 10.3390/W14203286.

[16] M. Yaseen, G. Nabi, M. Latif, and C. Author, "Assessment of Climate Change at Spatiao-Temporal Scales and its Impact on Stream Flows in Mangla Watershed," Pakistan J. Eng. Appl. Sci., vol. 15, pp. 17–36, 2014, Accessed: Jun. 16, 2024. [Online]. Available: https://journal.uet.edu.pk/ojs_old/index.php/pjeas/article/view/91

[17] M. J. Butt, R. Mahmood, and A. Waqas, "Sediments deposition due to soil erosion in the watershed region of Mangla Dam," Environ. Monit. Assess., vol. 181, no. 1–4, pp. 419–429, Oct. 2011, doi: 10.1007/S10661-010-1838-0/METRICS.

[18] M. Azmat, F. Laio, and D. Poggi, "Estimation of water resources availability and mini-hydro productivity in high-altitude scarcely-gauged watershed," Water Resour. Manag., vol. 29, no. 14, pp. 5037–5054, Nov. 2015, doi: 10.1007/S11269-015-1102-Z/METRICS.

[19] K. M. Kent, "NATIONAL ENGINEERING HANDBOOK SECTION 4 HYDROLOGY CHAPTER 15. TRAVEL TIME, TIME OF CONCENTRATION. AND LAG".

[20] H. Mckeever, V., Owen, W., Rallison, R., Engineers, "NATIONAL ENGINEERING HANDBOOK SECTION 4".

[21] H. Sutradhar and W.-C. Liu, "Surface Runoff Estimation Using SCS-CN Method in Siddheswari River Basin, Eastern India," J. Geogr. Environ. Earth Sci. Int., vol. 17, no. 2, pp. 1–9, Sep. 2018, doi: 10.9734/JGEESI/2018/44076.

[22] S. Satheeshkumar, S. Venkateswaran, and R. Kannan, "Rainfall–runoff estimation using SCS–CN and GIS approach in the Pappiredipatti watershed of the Vaniyar sub basin, South India," Model. Earth Syst. Environ. 2017 31, vol. 3, no. 1, pp. 1–8, Feb. 2017, doi: 10.1007/S40808-017-0301-4.

[23] N. N. . Vannasy M., "Estimating Direct Runoff from Storm Rainfall Using NRCS Runoff Method and GIS Mapping in Vientiane City, Laos", [Online]. Available:

http://article.nadiapub.com/IJGDC/vol9_no4/23.pdf

[24] C. Strapazan, I. A. Irimuş, G. Şerban, T. C. Man, and L. Sassebes, "Determination of Runoff Curve Numbers for the Growing Season Based on the Rainfall–Runoff Relationship from Small Watersheds in the Middle Mountainous Area of Romania," Water 2023, Vol. 15, Page 1452, vol. 15, no. 8, p. 1452, Apr. 2023, doi: 10.3390/W15081452.

[25] S. K. Mishra, M. K. Jain, P. Suresh Babu, K. Venugopal, and S. Kaliappan, "Comparison of AMC-dependent CN-conversion formulae," Water Resour. Manag., vol. 22, no. 10, pp. 1409–1420, Jan. 2008, doi: 10.1007/S11269-007-9233-5/METRICS.

[26] S. K. Mishra, R. P. Pandey, M. K. Jain, and V. P. Singh, "A rain duration and modified AMC-dependent SCS-CN procedure for long duration rainfall-runoff events," Water Resour. Manag., vol. 22, no. 7, pp. 861–876, Jul. 2008, doi: 10.1007/S11269-007-9196-6/METRICS.

[27] R. Amutha and P. Porchelvan, "Estimation of surface runoff in malattar sub-watershed using SCS-cn method," J. Indian Soc. Remote Sens., vol. 37, no. 2, pp. 291–304, Oct. 2009, doi: 10.1007/S12524-009-0017-7/METRICS.

[28] H. Blanco-Canqui and R. Lal, "Soil Resilience and Conservation," Princ. Soil Conserv. Manag., pp. 425–447, 2010, doi: 10.1007/978-1-4020-8709-7_16.

[29] E. Walker and V. Venturini, "Land surface evapotranspiration estimation combining soil texture information and global reanalysis datasets in Google Earth Engine," Remote Sens. Lett., vol. 10, no. 10, pp. 929–938, Oct. 2019, doi: 10.1080/2150704X.2019.1633487.

[30] M. Shahid et al., "Assessing the potential and hydrological usefulness of the CHIRPS precipitation dataset over a complex topography in Pakistan," Hydrol. Sci. J., vol. 66, no. 11, pp. 1664–1684, Aug. 2021, doi: 10.1080/02626667.2021.1957476.

[31] F. J. Tapiador et al., "Global precipitation measurement: Methods, datasets and applications," Atmos. Res., vol. 104–105, pp. 70–97, Feb. 2012, doi: 10.1016/J.ATMOSRES.2011.10.021.

[32] G. J. Huffman et al., "Integrated Multi-satellite Retrievals for the Global Precipitation Measurement (GPM) Mission (IMERG)," Adv. Glob. Chang. Res., vol. 67, pp. 343–353, 2020, doi: 10.1007/978-3-030-24568-9_19.

[33] C. Kummerow et al., "The Status of the Tropical Rainfall Measuring Mission (TRMM) after Two Years in Orbit," J. Appl. Meteorol. Climatol., vol. 39, no. 12, pp. 1965–1982, Dec. 2000, doi: 10.1175/1520-0450(2001)040.

[34] R. Jain, S., Jaiswal, R. K., Lohani, A. K., Galkate, "Development of cloud-based rainfall-run-off model using Google Earth Engine," 2021, [Online]. Available: https://www.currentscience.ac.in/Volumes/121/11/1433.pdf

[35] Z. Shen et al., "Recent global performance of the Climate Hazards group Infrared Precipitation (CHIRP) with Stations (CHIRPS)," J. Hydrol., vol. 591, p. 125284, Dec. 2020, doi: 10.1016/J.JHYDROL.2020.125284.

[36] J. S. Theon, "The tropical rainfall measuring mission (TRMM)," Adv. Sp. Res., vol. 14, no. 3, pp. 159–165, Mar. 1994, doi: 10.1016/0273-1177(94)90210-0.

[37] M. Babur, M. S. Babel, S. Shrestha, A. Kawasaki, and N. K. Tripathi, "Assessment of Climate Change Impact on Reservoir Inflows Using Multi Climate-Models under RCPs—The Case of Mangla Dam in Pakistan," Water 2016, Vol. 8, Page 389, vol. 8, no. 9, p. 389, Sep. 2016, doi: 10.3390/W8090389.

[38] Y. T. Dile and R. Srinivasan, "Evaluation of CFSR climate data for hydrologic prediction in data-scarce watersheds: an application in the Blue Nile River Basin," JAWRA J. Am. Water

Resour. Assoc., vol. 50, no. 5, pp. 1226–1241, Oct. 2014, doi: 10.1111/JAWR.12182.

[39] D. R. Fuka, M. T. Walter, C. Macalister, A. T. Degaetano, T. S. Steenhuis, and Z. M. Easton, "Using the Climate Forecast System Reanalysis as weather input data for watershed models," Hydrol. Process., vol. 28, no. 22, pp. 5613–5623, Oct. 2014, doi: 10.1002/HYP.10073.

[40] S. J. Bhuyan, K. R. Mankin, and J. K. Koelliker, "WATERSHED–SCALE AMC SELECTION FOR HYDROLOGIC MODELING," Trans. ASAE, vol. 46, no. 2, pp. 303-, Mar. 2003, doi: 10.13031/2013.12981.

[41] N. Y. Krakauer, T. Lakhankar, and G. H. Dars, "Precipitation Trends over the Indus Basin," Clim. 2019, Vol. 7, Page 116, vol. 7, no. 10, p. 116, Sep. 2019, doi: 10.3390/CLI7100116.

[42] A. P. Dimri et al., "Western Disturbances: A review," Rev. Geophys., vol. 53, no. 2, pp. 225–246, 2015, doi: 10.1002/2014RG000460.

[43] M. S. Hussain and S. Lee, "Investigation of summer monsoon rainfall variability in Pakistan," Meteorol. Atmos. Phys., vol. 128, no. 4, pp. 465–475, Aug. 2016, doi: 10.1007/S00703-015-0423-Z/METRICS.

[44] M. Adnan et al., "Variability and Predictability of Summer Monsoon Rainfall over Pakistan," Asia-Pacific J. Atmos. Sci., vol. 57, no. 1, pp. 89–97, Feb. 2021, doi: 10.1007/S13143-020-00178-2/METRICS.

[45] H. M. B. Wang, Y., "Application of the SCSCN method on runoff estimation in small watershed on Loess Plateau," Sci. Soil Water Conserv., vol. 6, no. 6, pp. 87–91, 2008.

[46] H. Tamiminia, B. Salehi, M. Mahdianpari, L. Quackenbush, S. Adeli, and B. Brisco, "Google Earth Engine for geo-big data applications: A meta-analysis and systematic review," ISPRS J. Photogramm. Remote Sens., vol. 164, pp. 152–170, Jun. 2020, doi: 10.1016/J.ISPRSJPRS.2020.04.001.